Coercivity of Domain Wall Motion in Thin Films of Amorphous Rare Earth–Transition Metal Alloys

M. MANSURIPUR,* R. C. GILES** and G. PATTERSON**
*Optical Sciences Center, University of Arizona, Tucson, Arizona 85721
**College of Engineering, Boston University, Boston, Massachusetts 02215

Computer simulations of a two-dimensional lattice of magnetic dipoles are performed on the Connection Machine. The lattice is a discrete model for thin films of amorphous rare earth–transition metal alloys, which have application as the storage media in erasable optical data storage systems. In these simulations the dipoles follow the dynamic Landau–Lifshitz–Gilbert equation under the influence of an effective field arising from local anisotropy, near-neighbor exchange, classical dipole–dipole interactions, and an externally applied field. Various sources of coercivity, such as defects and or inhomogeneities in the lattice, are introduced and the subsequent motion of domain walls in response to external fields is investigated.

Key words: coercivity, magnetization reversal

1. Introduction

Magnetization reversal in thin films of amorphous rare earth–transition metal (RE-TM) alloys is of considerable importance in erasable optical data storage.[1~13] The success of thermomagnetic recording and erasure depends on the reliable and repeatable reversal of magnetization in micron-size areas within the storage medium. A major factor usually encountered in descriptions of the thermomagnetic process is the coercivity of the magnetic medium. Coercivity, however, is an ill-defined concept generally used in the phenomenology of bulk reversal, but its usefulness and relevance to the phenomena occurring on the spatial/temporal scales of thermomagnetic recording are seriously in doubt. To begin with, there is the problem of distinguishing nucleation coercivity from the coercivity of wall motion. Then there is the question of speed and uniformity of motion as the wall expands beyond the site of its origination. Finally one must address the issues of stability and erasability—also intimately related to coercivity—in a framework wide enough to allow the consideration of local instability and partial erasure. It is fair to say that the existing models and or theories of coercivity[14~31] are generally incapable of handling the problems associated with thermomagnetic recording and erasure. In our view, the natural vehicle for conducting theoretical investigations in this area is dynamic computer simulations based on the fundamental concepts and equations of micromagnetics. We have conducted several such studies in the past[32~35] and have succeeded in clarifying some of the issues involved in the nucleation stage of the magnetization reversal process. Also treated in these studies were the dynamics of wall motion in homogeneous media. The purpose of the present paper is to investigate the coercivity of wall motion at the submicrometer scale and in the presence of defects and/or inhomogeneities, using large scale computer simulations.

The simulations were performed for a two dimensional hexagonal lattice of magnetic dipoles following the Landau–Lifshitz–Gilbert equation.[36] In addition to interacting with an externally applied field, the dipoles were subject to effective fields arising from local uniaxial anisotropy, nearest neighbor exchange, and long range dipole–dipole interactions. Details of the micromagnetic model have been previously published[32, 37~39] and will not be repeated here. Suffice it to say that the massive parallelism of the Connection Machine on which these simulations were performed, together with the fast Fourier transform algorithm[37, 38] which was used to compute the demagnetizing field, enabled us to accurately simulate a large (256 × 256) hexagonal lattice of dipoles.

Since the lattice constant was chosen to be 10Å in these simulations, the total area of the lattice corresponds to a section of the magnetic film with dimensions $L_x = 0.256\,\mu m$, $L_y = 0.222\,\mu m$. Periodic boundary conditions were imposed on the lattice in both X and Y directions, but the film thickness along Z was finite and the magnetization distribution in this direction was assumed to be uniform.

In a previous paper[7] where nucleation of reverse-magnetized domains was under consideration, it was shown that the fields required to initiate the reversal process in a uniform material are generally higher than those observed in practice. Various submicron-size "defects" were then introduced in the magnetic state of the lattice and the values of nucleation coercivity corresponding to different types, sizes, and strengths of these "defects" were computed. Voids, for instance, were found to have an insignificant effect on the value of the nucleation field, but reverse-magnetized seeds, formed and stabilized in areas with large local anisotropy, could substantially reduce the nucleation coercivity. Similarly, the presence of spatial variations in the magnetic parameters of the material, such as random axis anisotropy, was found to affect the coercivity of nucleation.

Random spatial fluctuations and structural/magnetic defects also create barriers to domain wall motion. These barriers are overcome only when sufficiently large magnetic fields (in excess of the so-called wall motion coercivity) are applied. Simulations reveal that wall coercivity in amorphous RE-TM alloy films is generally less than the corresponding nucleation coercivity. This finding is in agreement with the experimentally observed square shape of the hysteresis loops in these media. The strength of wall coercivity, of course, depends on the type and size of fluctuations and/or defects. The results reported in the next section are intended to clarify some of these relationships.

Magnetization-pattern-displays in this paper utilize a color coding scheme. Since the magnitude of the magnetization vector $\boldsymbol{M}$ will be fixed throughout the lattice, the *Color Sphere* is used to represent its local orientation. The Color Sphere is white at its north pole, black at its south pole, and covers the visible spectrum on its equator in the manner shown in Fig. 1. As one moves from the equator to the north pole on a great circle, the color pales, *i.e.*, it mixes with increasing amounts of white, until it becomes white at the pole. Moving towards the south pole has the opposite effect as the color mixes with increasing amounts of black. Thus, when the magnetization vector at a given site is perpendicular to the plane of the lattice and along the positive (negative) Z axis, its corresponding pixel will be white (black). For $\boldsymbol{M}$ in the plane of the lattice the pixel is red when pointing along $-X$, light green along $-Y$, blue along $+X$, and purple along $+Y$. In the same manner, other orientations of $\boldsymbol{M}$ map onto the corresponding color on the Color Sphere.

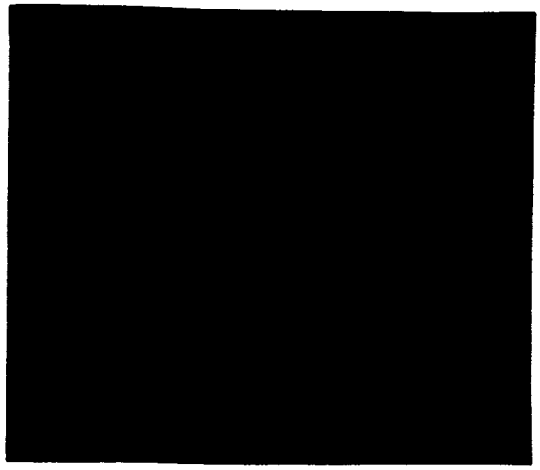

Fig. 1 The *Color Circle* is used to encode the direction of magnetization in the plane of the lattice. In this scheme a red pixel is associated with local magnetization direction along $-X$, light green corresponds to $-Y$, blue to $+X$, and purple to $+Y$. When a vector is not completely in the plane of the lattice, but has a perpendicular component along $+Z$ (or $-Z$), its associated color is obtained by mixing the color of its in-plane component with a certain amount of white (or black), the strength of white (or black) depending on the magnitude of the vertical component. A vector fully aligned with the $+Z$ direction is shown by a white pixel, while a vector in the $-Z$ direction is displayed as black.

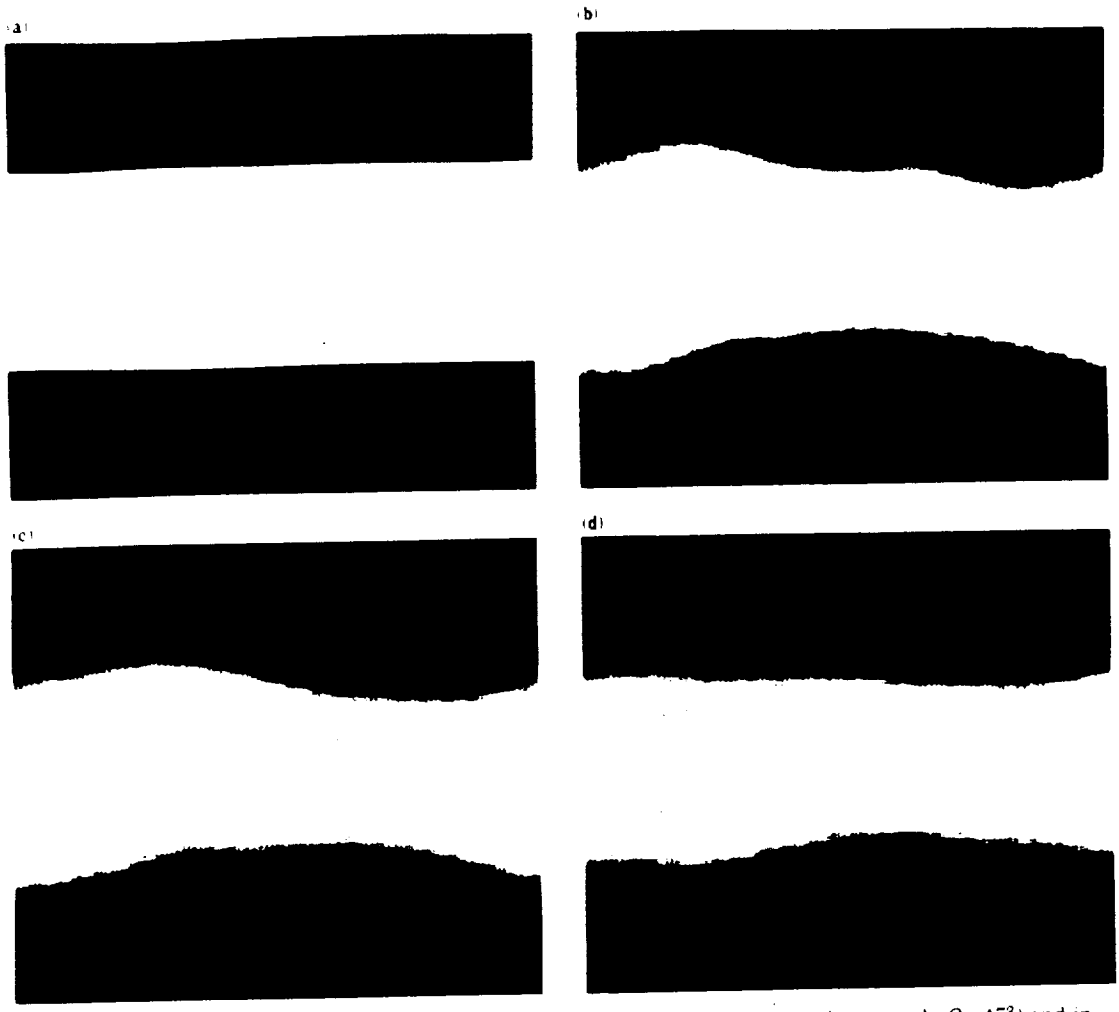

Fig. 2 Formation of domain walls in a medium with random axis anisotropy (cone angle $\Theta=45°$) and in the absence of an applied field. (a) Dipoles in the white region are initialized along $-Z$, while dipoles in the dark region are initialized along $-Z$. (b) The state of the lattice at $t=0.8$ ns. Each wall contains three vertical Bloch lines (VBLs) at this stage. (c) The state of the lattice at $t=1.7$ ns. The number of VBLs has not changed since the previous frame, but they have moved along the walls. (d) The steady state of the lattice at $t=4.56$ ns. The number of VBLs in each wall is still three.

2. Structure and Motion of Domain Walls

The following set of parameters (used in all simulations reported in this paper) are typical of amorphous films of TbFeCo used in magneto-optical recording: saturation magnetization $M_s=100$ emu/cm^3, anisotropy energy constant $K_u=10^6$ erg/cm^3, exchange stiffness coefficient $A_x=10^{-7}$ erg/cm, film thickness $h=500$Å, damping coefficient $\alpha=0.5$, and gyromagnetic ratio $\gamma=-10^7$ Hz/Oe. In subsequent discussions the term "random axis anisotropy" is meant to imply that the anisotropy axes of the lattice are distributed randomly and independently among the lattice cells (or among various groups of these cells). By keeping the deviation angle θ of the anisotropy axis from Z below a certain maximum angle Θ, the random assignment of axes preserves the perpendicular nature of the overall anisotropy. Thus θ is

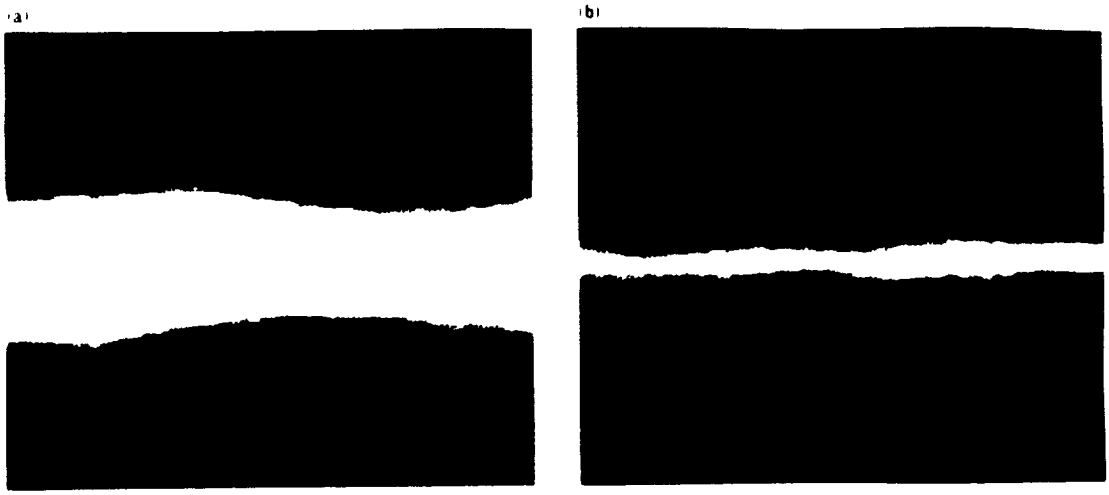

Fig. 3 Collapse of the stripe domain depicted in Fig. 2(d) under the external field $H_e = 1000$ Oe. Frames (a) and (b) show the state of the lattice at $t = 0.96$ ns and $t = 3.58$ ns, respectively.

Fig. 4 Patchy lattice with 346 patches. Colors are used solely for the purpose of identification of different patches, otherwise they have no meaning or significance.

selected with equal probability from the values in the interval $[0, \Theta]$; for brevity, Θ will be referred to as the *cone angle* in this paper. No constraints are imposed on the distribution of the azimuthal angle ϕ and its values are therefore selected (also randomly and independently) from the interval $[0, 360^\circ]$. It is perhaps worth mentioning at this point that the random assignment of the axes of anisotropy to individual dipoles does not automatically result in rapid variations of the direction of magnetization in space. In fact, the strong exchange field in our simulations gives rise to a smooth distribution of the magnetization vector across the lattice, even when large cone angles are involved.

Figure 2 shows the structure of domain walls in a uniform medium with the aforementioned set of parameters. The lattice for this set of simulations had random axis anisotropy over individual cells with a cone angle of $\Theta = 45^\circ$, that is, the axis of local anisotropy was selected randomly for each cell of the lattice with $\theta \in [0, 45^\circ]$, $\phi \in [0, 360^\circ]$, and the values of θ and ϕ chosen for one cell were independent of those selected for all the other cells. Initially the central band of the lattice was magnetized in the $-Z$ direction while the remaining part was magnetized in the $-Z$ direction, as shown in Fig. 2(a). When the lattice was allowed to relax for 0.8 ns, the pattern in Fig. 2 (b) was obtained. Notice that there are three vertical Bloch lines (2π VBLs) in each wall and that the walls are no longer straight. By allowing the lattice to relax for another 0.9 ns we obtained the pattern of Fig. 2(c), which shows significant VBL movements along the walls. Finally, Fig. 2(d) shows the steady state situation at $t = 4.56$ ns. Both walls are now straightened considerably, but the number of VBLs in each wall has not changed; no amount of relaxation can unwind a 2π Bloch line.

A perpendicular field H_z = 200 Oe, applied to the state of Fig. 2(d), moves the walls somewhat closer to each other, but fails to eliminate them. The force of demagnetization apparently opposes the external field in collapsing the reverse-magnetized stripe. The domain will collapse, however, under an applied field of H_z = 1000 Oe, as shown in Fig. 3. Frames (a) and (b) in this figure correspond, respectively, to t = 0.96 ns and t = 3.58 ns, where t is the elapsed time since the application of the field. Although not shown in this figure, the walls proceeded to collide and annihilated each other at a later time.

In the above example the randomness in the lattice parameters is clearly too weak to cause significant coercivity for the wall motion. To remedy this problem, we increased the fluctuations' correlation length by introducing large patches, that is, patches whose dimensions are large compared to the width of the domain wall. Figure 4 shows a typical lattice covered with 346 patches of random shape and size. These patches were created by selecting at random a number of lattice sites as seeds, and growing outward from them (in a random fashion) until every site in the lattice belonged to one patch or another. By assigning different attributes to different patches one can thus create spatial variations in the structure magnetic properties of the lattice over length ales comparable to the average patch size.

Figure 5(a) shows a stripe of reverse magnetization in the patchy lattice of Fig. 4. For the sake of clarity, the boundaries of the patches are highlighted in the figure. Each patch is assigned an axis of anisotropy, randomly and independently of all the other patches, with a cone angle of Θ=45°. The walls in Fig. 5 are somewhat more jagged than those in Fig. 2, where the patches were essentially the size of an individual lattice cell. Under an applied field of H_z = − 1.5 kOe the walls in Fig. 5(a) moved slightly and then came to equilibrium as shown in Fig. 5(b). A plot of $\langle M_z \rangle$, the average magnetization of the lattice along the Z axis, *versus* time is shown in Fig. 5(c). This plot indicates that the initial $\langle M_z \rangle$, which is slightly above zero, has increased to about 20% of its saturation value in the first 0.5 ns after the application of the field, but has stopped growing at the point. Compare this situation with that depicted in Figs. 2 and 3, where 1 kOe of field was sufficient to annihilate the walls. Clearly it is the presence of patches and not the demagnetizing force which is responsible for blocking the wall motion. Thus the wall motion coercivity has increased as a result of increased correlation among the local easy axes. When the field was further increased to H_z = 2 kOe, it became possible to push the walls beyond the barriers and force them to collide and disappear. (Because of the periodic boundary condition, the walls collide after wrapping around the lattice.) Figure 5(d) shows an advanced state of domain expansion under the 2 kOe field (t = 1.154 ns). Note that the lower wall has remained almost intact, while the upper wall has moved substantially. The plot of $\langle M_z \rangle$ *versus* time in Fig. 5(e), starting with the application of the 2 kOe field, reveals that the movement is slow in the beginning, as the field struggles to overcome the pinning of the walls. Once released, the wall moves rapidly for a period of about 1 ns until either another pinning occurs or the demagnetization force begins to push the walls apart (remember the periodic boundary condition). In any event, the motion slows down at t = 1.2 ns and the growth rate of $\langle M_z \rangle$ drops by nearly a factor of 2. The walls, however, continue to move out, wrap around at the boundary, and eventually annihilate.

In order to understand the effect of patch size on coercivity, we repeated the preceding simulation for another lattice which had the same set of parameters as the lattice in Fig. 5, but whose total number of patches had increased to 1300. Again we found that H_z = 1.5 kOe could not move the walls significantly, but that H_z = 2 kOe could. It is probably safe, therefore, to assert that the average size of the patch does not affect the coercivity in a substantial way, so long as it is larger than the characteristic width of the domain wall in the given medium.

Figure 6(a) shows another strip of reverse magnetization in the patchy lattice of Fig. 4. This time, however, a few of the patches have been made void by assigning the value of zero to their magnetic parameters. These void patches are shown as gray regions in the figure. (No special property is assumed

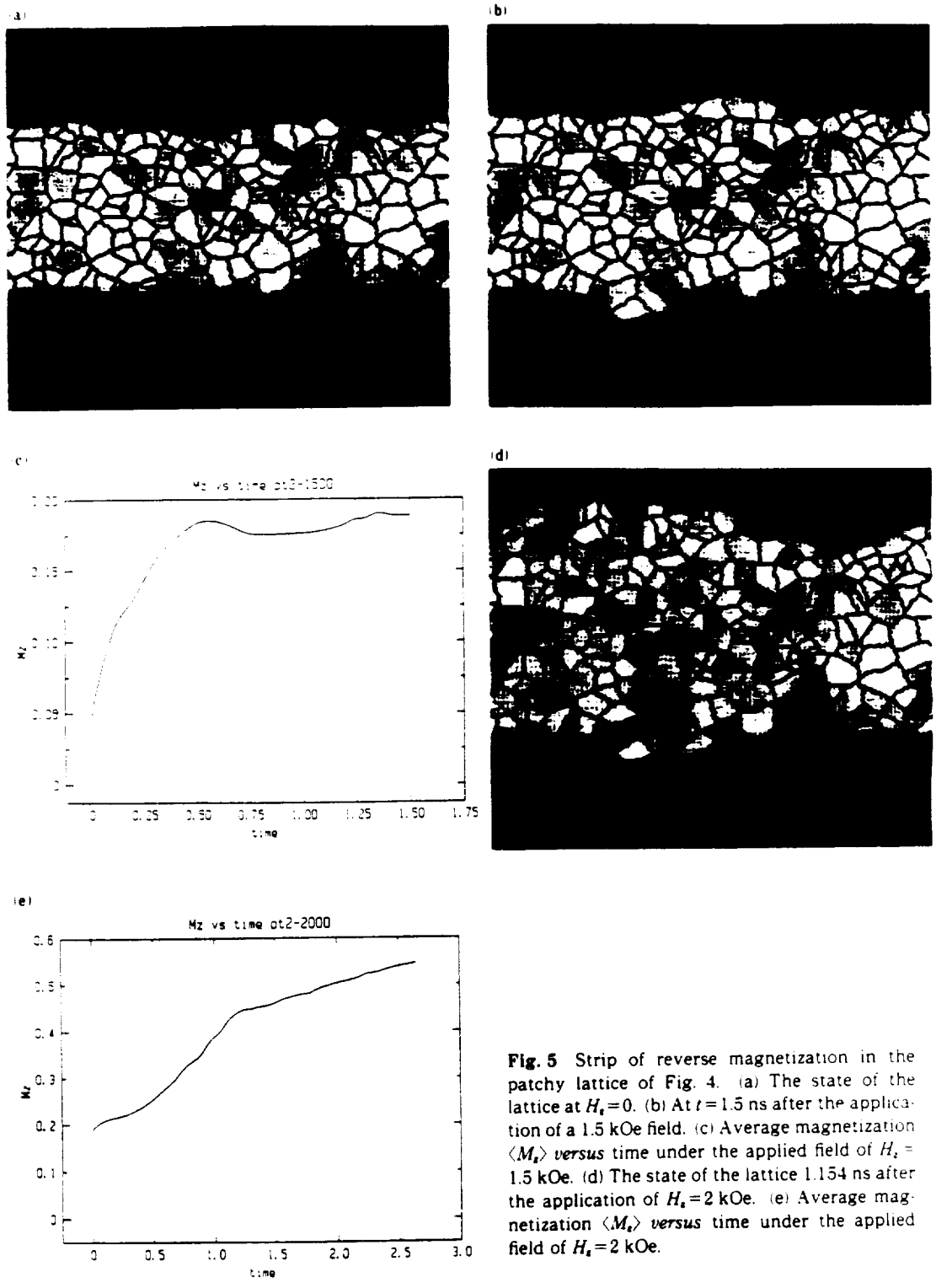

Fig. 5 Strip of reverse magnetization in the patchy lattice of Fig. 4. (a) The state of the lattice at $H_z=0$. (b) At $t=1.5$ ns after the application of a 1.5 kOe field. (c) Average magnetization $\langle M_z \rangle$ *versus* time under the applied field of $H_z=1.5$ kOe. (d) The state of the lattice 1.154 ns after the application of $H_z=2$ kOe. (e) Average magnetization $\langle M_z \rangle$ *versus* time under the applied field of $H_z=2$ kOe.

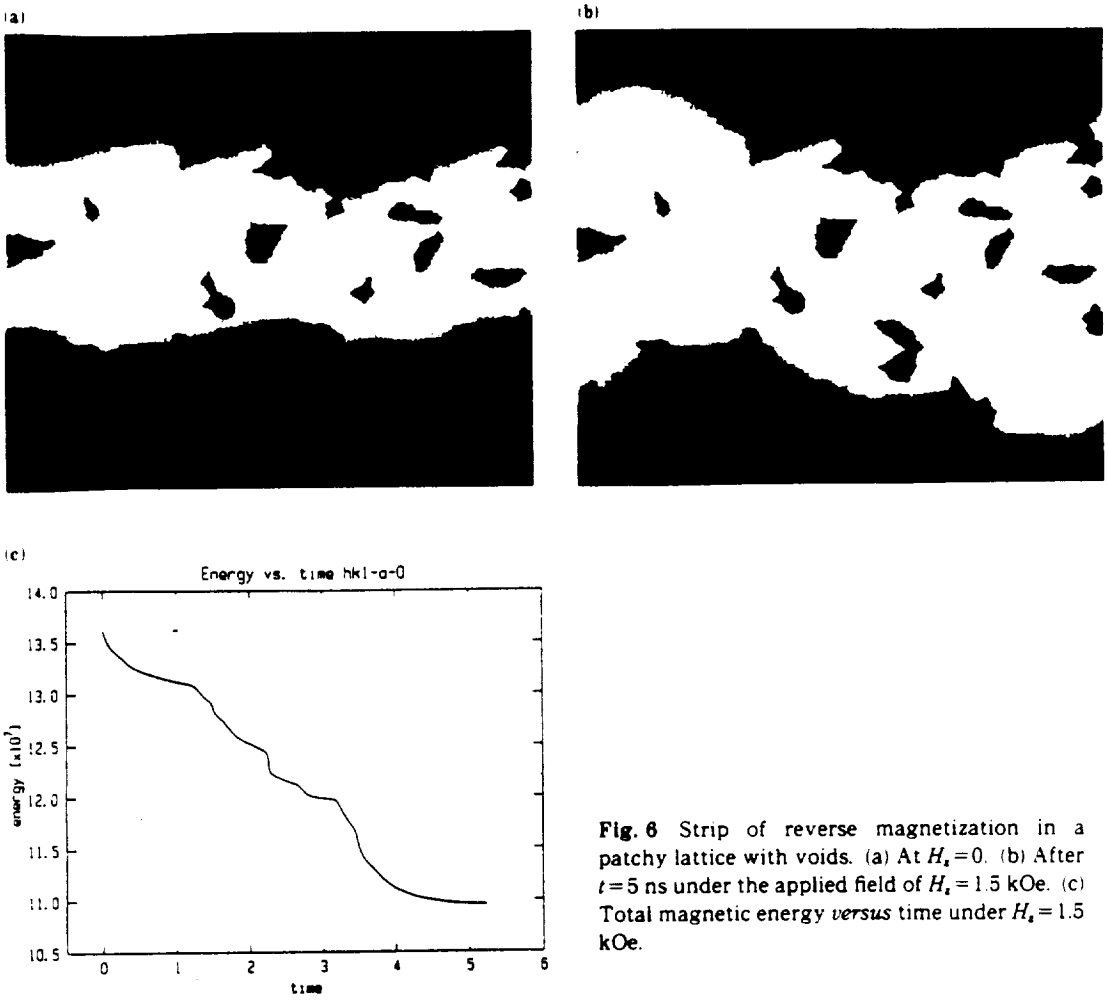

Fig. 6 Strip of reverse magnetization in a patchy lattice with voids. (a) At $H_a = 0$. (b) After $t = 5$ ns under the applied field of $H_a = 1.5$ kOe. (c) Total magnetic energy *versus* time under $H_a = 1.5$ kOe.

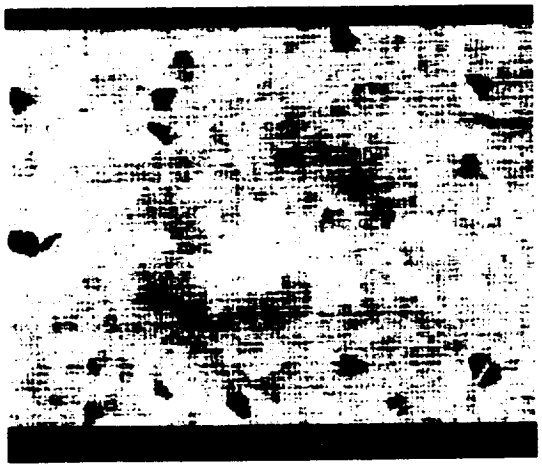

Fig. 7 Lattice with 662 patches, of which 24 are "defective". A normal patch is assigned anisotropy axis within a cone of $\Theta = 10°$ from the perpendicular direction, whereas the easy axis of a defective patch is nearly in the plane of the lattice. The color coding scheme depicts the direction of anisotropy for the individual patches.

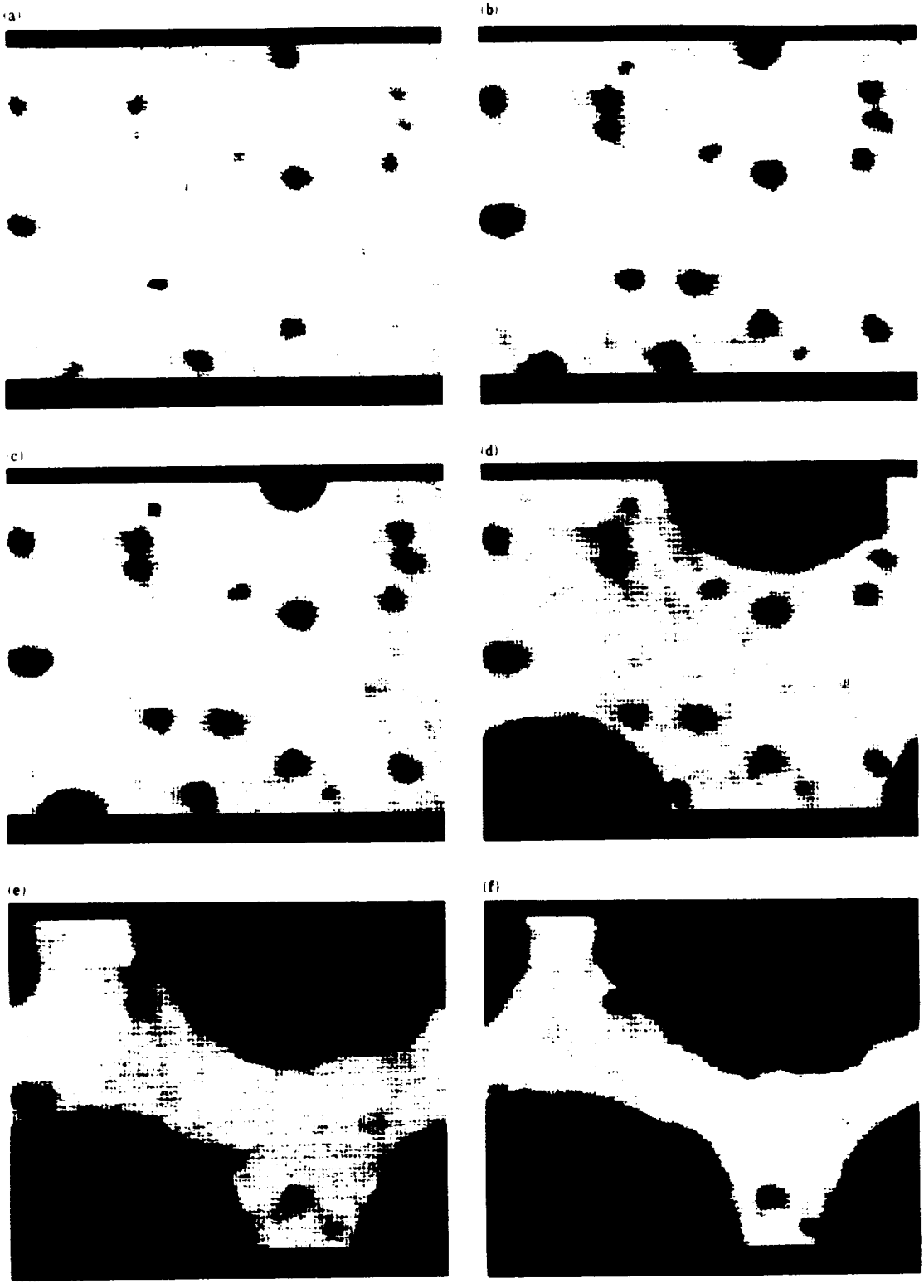
(a)
(b)
(c)
(d)
(e)
(f)

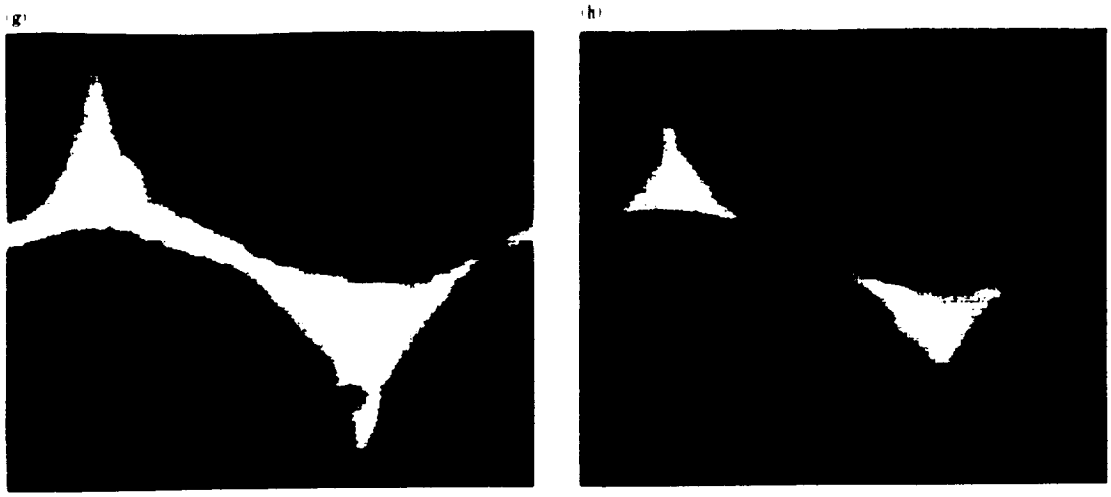

Fig. 8 Magnetization distribution in the patchy lattice of Fig. 7. (a) The remanent state at $H_z = 0$. (b) The steady state under $H_z = -8900$ Oe. The remaining frames show the time evolution of the lattice under $H_z = -8920$ Oe. (c) At $t = 0.24$ ns the reversal is underway with a nucleus forming in the lower left corner. The periodic extension of this nucleus in the upper right corner of the lattice is also visible. (d) At $t = 0.72$ ns. (e) At $t = 1$ ns. (f) At $t = 1.08$ ns. (g) At $t = 1.248$ ns. (h) At $t = 1.32$ ns.

for the dipoles at the void boundaries, their magnetic parameters being the same as those elsewhere in the lattice. Of course no exchange field is exerted on the boundary dipoles from the neighboring cells on the void side, and the magnetic charges that accumulate on the void boundaries are automatically accounted for when the demagnetizing field is computed.) The remaining patches are all identical in their magnetic properties except for the value of the anisotropy constant K_u which fluctuates randomly and independently from patch to patch. (The standard deviation of these fluctuations is 20% of the average value of K_u.) No other spatial variations in the parameters have been assumed and, in particular, all axes of anisotropy are perpendicular (*i.e.*, $\Theta = 0$).

The walls in Fig. 6(a) have automatically adjusted themselves to minimize their lengths by attaching to the voids in the neighborhood. Minimization of length is tantamount to minimization of total wall energy and is therefore favored by the magnetic system under consideration. Figure 6(b) shows the state of the lattice under an applied field of $H_z = +1.5$ kOe at $t \simeq 5$ ns. Apparently, the walls have continued to seek voids to attach onto, while expanding in response to the external field. Figure 6(c) is a plot of the total magnetic energy of the lattice during this growth period. It is marked by slow declines, characteristic of continuous wall motion, and rapid drops, corresponding to detachments from or attachments to the voids. It is thus observed that void-like defects in real media can create jagged domain boundaries, increase the coercivity of wall motion, and cause discontinuities in the propagation process.

As another example consider the case of a patchy lattice with a different kind of "defect". The 662 patches in this case were divided into two groups as shown in Fig. 7. The first group, consisting of 638 patches, were assigned nearly-perpendicular axes of anisotropy, as has been our practice so far. Each one of the patches in this group was assigned an axis, randomly and independently of the others, with a cone angle of $\Theta = 10°$. The second group of 24 patches were assigned axes of anisotropy that were nearly parallel to the plane of the lattice. The randomly and independently chosen values of θ and ϕ for these patches belonged to the intervals $[80°, 90°]$ and $[0, 360°]$, respectively. (In the color-coded distribution of the anisotropy axes shown in Fig. 7, the

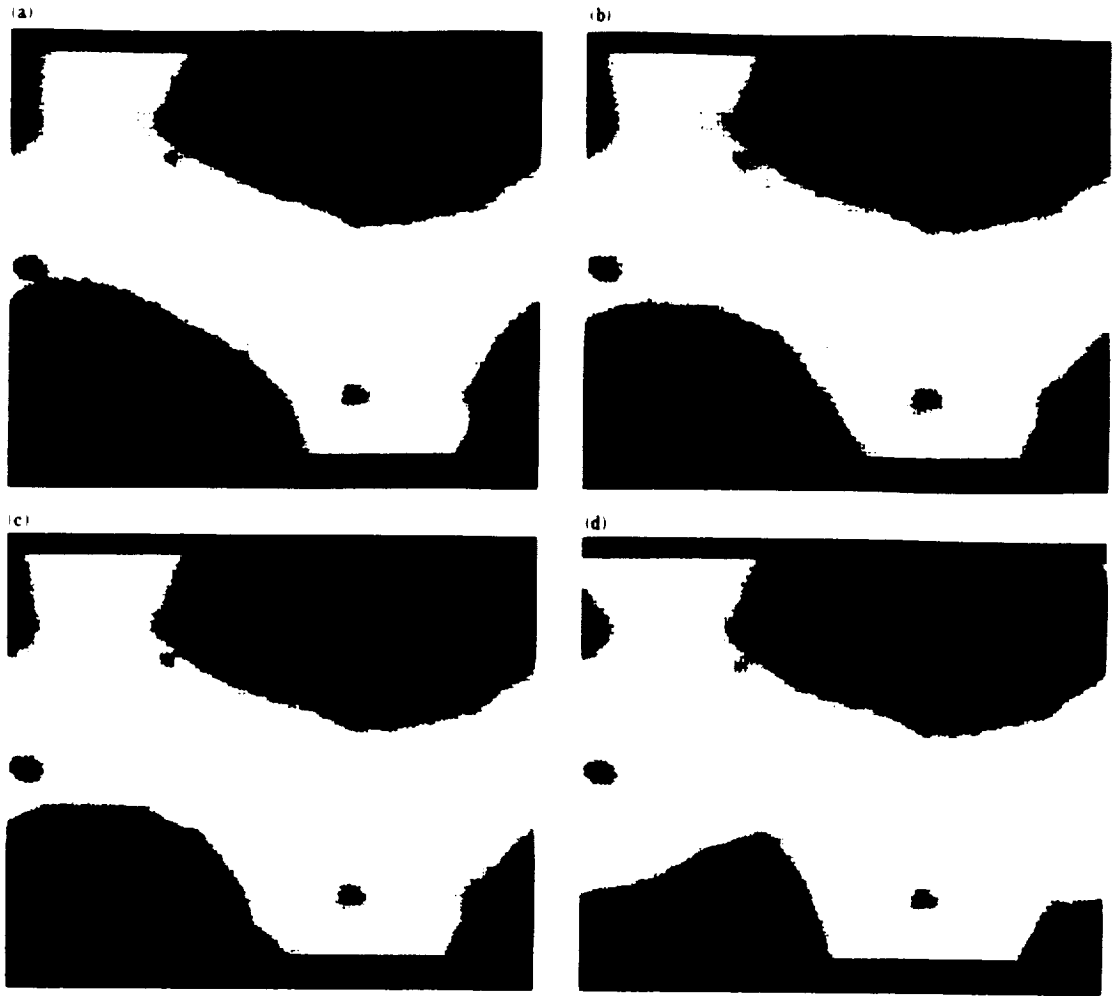

Fig. 9 Evolution of the magnetization state of Fig. 8(e) after the removal of the external field. (a) $t = 0.44$ ns. (b) $t = 1.12$ ns. (c) $t = 1.16$ ns. (d) $t = 5.83$ ns.

patches with prominent colors are those with nearly in-plane axes.) The remaining parameters of the lattice were the same as before. In the following discussion this lattice shall be referred to as "the lattice with in-plane defects".

The entire lattice with in-plane defects was initially saturated along the $+Z$ axis and then allowed to relax in zero field, until the remanent state of magnetization, shown in Fig. 8(a), was arrived at. The strong exchange interaction has clearly forced the magnetization of the in-plane patches towards the $-Z$ axis, but the tendency towards the plane is still visible in some areas. We subjected the remanent state to a reverse-magnetizing external field along $-Z$, and searched for the critical magnitude of this field that would initiate the reversal process. The critical field for nucleation was found to be 8910 Oe. It is important to note that in the absence of the in-plane patches the same sample had a nucleation coercivity close to 18 kOe. The in-plane regions, therefore, facilitate the nucleation process. In Fig. 8 (b) we show the pattern of magnetization distribution under an applied field $H_z = -8900$ Oe, which is only slightly weaker than the critical field. The defects are seen to have been pushed toward the plane, yet the field is not quite strong enough to

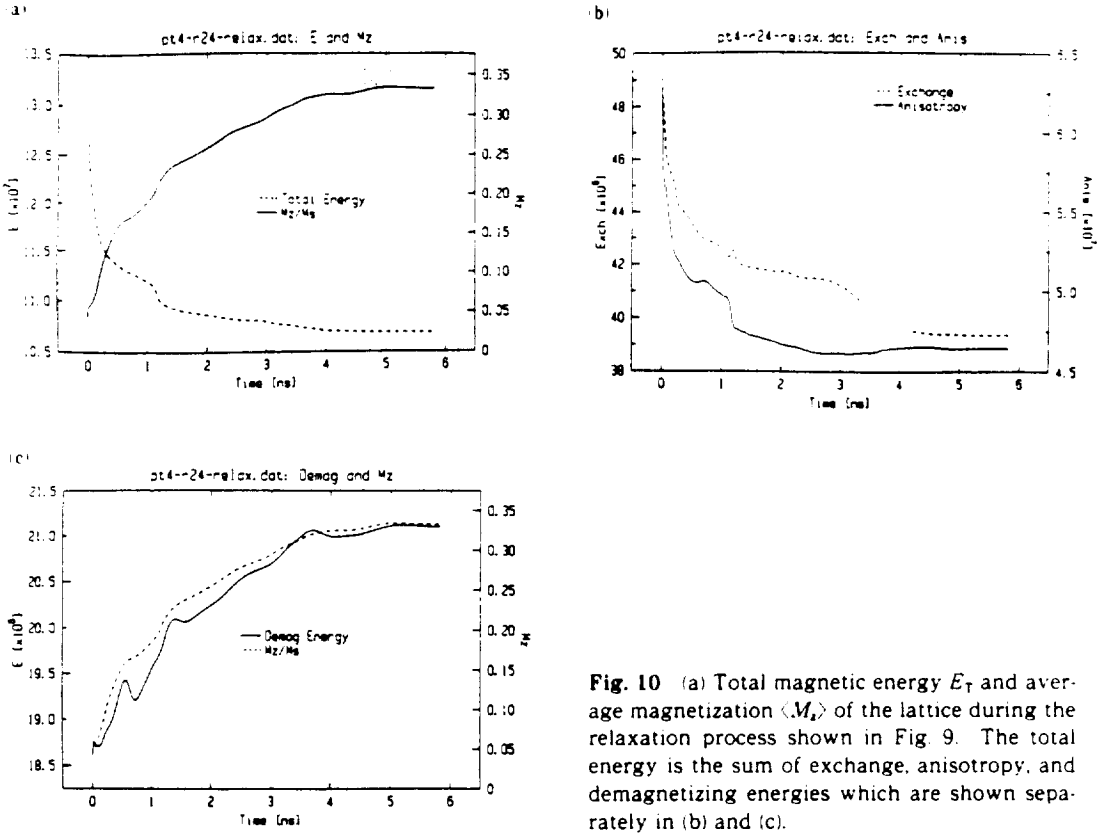

Fig. 10 (a) Total magnetic energy E_T and average magnetization $\langle M_z \rangle$ of the lattice during the relaxation process shown in Fig. 9. The total energy is the sum of exchange, anisotropy, and demagnetizing energies which are shown separately in (b) and (c).

cause them to reverse. When the field was raised to $H_z = -8920$ Oe, the reversal began, as the time evolution series in Figs. 8(c) to 8(h) shows. First the defect at the lower left corner of the lattice (with its periodic extension at the upper right) nucleated. Then the nucleus grew until the entire sample was reverse-magnetized. Note how the defects seem to attract the domain wall as it approaches them, and then try to pin the wall to prevent its further progress. The applied field, however, is strong enough to overcome the pinning of the wall and bring the reversal to completion. A hysteresis loop with high squareness is the hallmark of this type of reversal.

In order to investigate the pinning process and the phenomenon of wall coercivity, we took the state of the lattice in Fig. 8(e) as the initial state for another simulation and set the external field to zero. Note that because of the periodic boundary condition imposed on the hexagonal lattice, the several black regions in Fig. 8(e) are in fact different pieces of one and the same reverse-magnetized domain. This (roughly circular) domain must begin to collapse immediately after the removal of the external field. The reason for the collapse is that the domain wall energy density of the material ($\sigma_w = 4\sqrt{A_x K_u} = 1.265$ erg/cm^2) is greater than the demagnetizing energy density at the wall ($\sim 6\pi h M_s^2 = 0.943$ erg/cm^2) and, therefore, energy minimization favors the shrinking of the domain. Figure 9 shows the time evolution of the shrinking process, with frames (a) to (d) corresponding to $t = 0.44$ ns, 1.12 ns, 1.16 ns, and 5.83 ns after the external field is reset to zero. In the absence of defects the collapse would have been complete, but in the present situation after an initial period of shrinking, the defects trap the domain wall and prevent its collapse. Note in Fig. 9(c), for instance, how

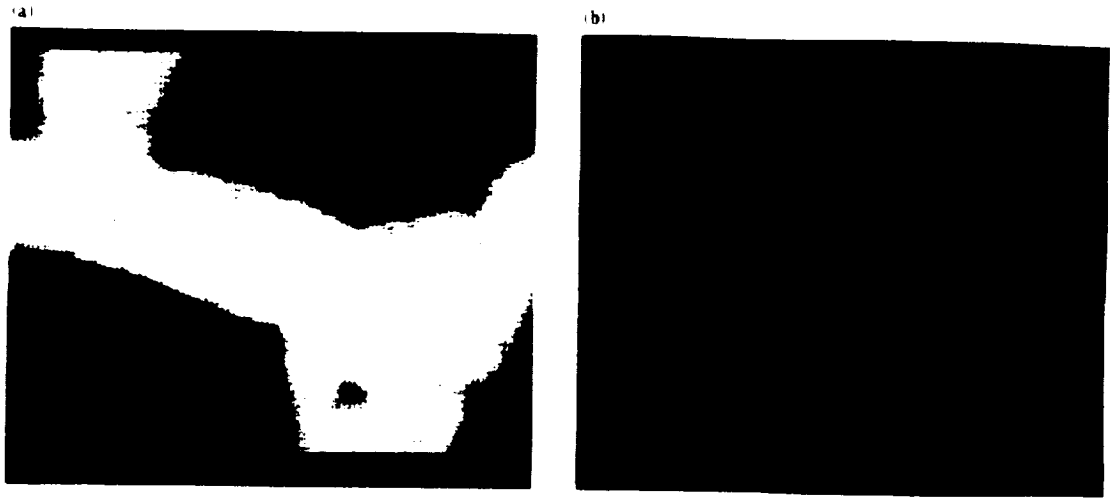

Fig. 11 (a) Magnetization distribution pattern corresponding to the relaxation of the state in Fig. 8(f) under zero applied field. The steady state shown here is obtained after 4 ns of relaxation. (b) Dot product of the initial state of magnetization shown in Fig. 8(f) and the final (relaxed) state shown in Fig. 11(a). The color coding scheme for this figure which is different from that used elsewhere in the paper is described in the text.

the defect in the lower central part of the lattice attracts the wall and keeps it pinned there afterwards. Therefore, like the other types of defect described in previous examples, defects with in-plane anisotropy are likely responsible for the observed wall coercivity of the RE-TM media. A comparison of Fig. 9(d) with Fig. 7 clearly indicates that the domain is fully anchored on a number of defects. The fact that the domain in Fig. 9(d) is stable has practical significance in data storage applications, since it provides one possible mechanism for the stability of very small thermomagnetically recorded marks.

Figure 10 shows plots of energy E and average magnetization $\langle M_z \rangle$ during the relaxation process depicted in Fig. 9. As expected, the total energy E_{TOT} of the system decreases in time, while the average magnetization along Z increases. A sudden jump in the curve of energy (such as the one at $t \simeq 1.14$ ns) is an indicator of the capture of the wall by a defect. Plots of the various components of energy in Figs. 10 (b) and 10(c) show that the exchange and anisotropy energies of the system generally decrease with time, while the demagnetizing energy increases. This is to be expected of course in the present situation since, as was pointed out earlier, during relaxation the total length of the domain wall must decrease.

Finally, starting from the state of Fig. 8(f), we show in Fig. 11 the result of relaxation under zero applied field. The magnetization pattern in Fig. 11(a) is the steady state of the lattice obtained after 4 ns of relaxation. The reverse domain here is somewhat larger than the one in Fig. 9(d), simply because it started from a larger initial domain. The jaggedness of the wall in Fig. 11(a) is particularly striking. Figure 11 (b) shows the difference between the initial state in Fig. 8(f) and the final relaxed state in Fig. 11(a), using a different color coding scheme. What is depicted here is the dot product between the magnetization directions of the initial and final states: each pixel represents a scalar value in the interval $[-1, +1]$ corresponding to the dot product of the two unit vectors. In this coloring scheme $+1$ corresponds to purple, -1 to red, and the values in between are mapped continuously to the color wheel of Fig. 1. Figure 11(b) clearly shows the nonuniform motion of the wall during zero-field relaxation. While some regions of the wall have not moved at all, others have travelled by as much as a few hundred angstroms. In general, the wall seems to have remained pinned on

several defects, while regions of the wall in between those defects have relaxed toward a state of minimum energy. Once again, the observed behavior confirms that small patches of material with in-plane anisotropy are effective in capturing and stabilizing the small domains.

3. Concluding Remarks

Hypothetical mechanisms of wall coercivity in thin films of amorphous rare earth-transition metal alloys were examined in this paper. Using computer simulations, we found that regions as small as a few hundred angstroms in diameter, with certain deviations of their structure magnetic attributes from the rest of the film, could trap domain walls and cause significant changes in the value of the coercive field. Values of the coercive field obtained by simulation are comparable to those observed in practice. Whether or not these hypothetical sources exist in real materials is a question whose answer must await further progress in experimental "nanomagnetics". Among the existing tools for observation of the magnetic state in thin films, Lorentz Electron Microscopy[40] and Magnetic Force Microscopy[41] have the potential to clarify this situation in the near future.

Acknowledgements

This work has been made possible by grants from the IBM Corporation and, in part, by support from the Optical Data Storage Center at the University of Arizona.

References

1) P. Hansen and H. Heitmann, *IEEE Trans. Magn.* **MAG-25**, 4390 (1989).
2) P. Chaudhari, J. J. Cuomo and R. J. Gambino, *Appl. Phys. Lett.*, **22**, 337 (1973).
3) R. J. Gambino, P. Chaudhari and J. J. Cuomo, AIP Conf. Proc. No. **18, Pt. 1**, pp. 578-592 (1973).
4) T. Chen, D. Cheng and G. B. Charlan, *IEEE Trans. Magn.* **MAG-16**, 1194 (1980).
5) Y. Mimura, N. Imamura and T. Kobayashi, *IEEE Trans. Magn.* **MAG-12**, 779 (1976).
6) Y. Mimura, N. Imamura, T. Kobayashi, A. Okada and Y. Kushiro, *J. Appl. Phys.*, **49**, 1208 (1978).
7) F. E. Luborsky, *J. Appl. Phys.*, **57**, 3592 (1985).
8) H. Tsujimoto, M. Shouji, A. Saito, S. Matsushita and Y. Sakurai, *J. Magn. Magn. Materials*, **35**, 139 (1983).
9) G. A. N. Connell, R. Allen and M. Mansuripur, *J. Appl. Phys.*, **53**, 7759 (1982).
10) M. Urner-Wille, P. Hansen and K. Witter, *IEEE Trans. Magn.* **MAG-16**, 1188 (1980).
11) T. C. Anthony, J. Burg, S. Naberhuis and H. Birecki, *J. Appl. Phys.*, **59**, 213 (1986).
12) Y. Sakurai and K. Onishi, *J. Magn. Magn. Materials*, **35**, 183 (1983).
13) P. Wolniansky, S. Chase, R. Rosenvold, M. Ruane and M. Mansuripur, *J. Appl. Phys.*, **60**, 346 (1986).
14) E. C. Stoner and E. P. Wohlfarth, *Phil. Trans. Roy. Soc.*, **A240**, 599 (1948).
15) D. O. Smith, *J. Appl. Phys.*, **29**, 264 (1958).
16) E. M. Bradley and M. Prutton, *J. Electronics and Control*, **6**, 81 (1959).
17) S. Middelhoek, PhD Thesis, University of Amsterdam (1961).
18) R. Harris, M. Plischke and M. J. Zuckermann, *Phys. Rev. Lett.*, **31**, 160 (1973).
19) R. Harris, S. H. Sung and M. J. Zuckermann, *IEEE Trans. Magn.* **MAG-14**, 725 (1978).
20) R. Friedberg and D. I. Paul, *Phys. Rev. Lett.*, **34**, 1234 (1975).
21) D. I. Paul, *Phys. Lett.*, **64A**, 485 (1978).
22) D. I. Paul, *J. Appl. Phys.*, **53**, 2362 (1982).
23) B. K. Middelton, "Magnetic Thin Films and Devices", in "Active and Passive Thin Film Devices", ed. by T. J. Coutts, Academic Press, New York (1978), Chapter 11.
24) A. Sukiennicki and E. Della Torre, *J. Appl. Phys.*, **55**, 3739 (1984).
25) K. Ohashi, H. Tsuji, S. Tsunashima and S. Uchiyama, *Jpn. J. Appl. Phys.*, **19**, 1333 (1980).
26) K. Ohashi, H. Takagi, S. Tsunashima, S. Uchiyama and T. Fujii, *J. Appl. Phys.*, **50**, 1611 (1979).
27) M. C. Chi and R. Alben, *J. Appl. Phys.*, **48**, 2987 (1977).
28) J. M. D. Coey, *J. Appl. Phys.*, **49**, 1646 (1978).
29) J. M. D. Coey and D. H. Ryan, *IEEE Trans. Magn.* **MAG-20**, 1278 (1984).
30) E. Callen, Y. J. Liu and J. R. Cullen, *Phys. Rev. B*, **16**, 263 (1977).
31) R. C. O'Handley, *J. Appl. Phys.*, **62**, R15 (1987).
32) M. Mansuripur, *J. Appl. Phys.*, **63**, 5809 (1988).
33) M. Mansuripur and T. W. McDaniel, *J. Appl. Phys.*, **63**, 3831 (1988).
34) M. Mansuripur and R. Giles, *Computers in Physics*, **4**, 291 (1990).
35) R. Giles and M. Mansuripur, submitted to *Computers in Physics*.
36) A. P. Malozemoff and J. C. Slonczewski, "Magnetic Domain Walls in Bubble Materials", Academic Press, New York (1979).
37) M. Mansuripur and R. Giles, *IEEE Trans. Magn.* **MAG-24**, 2326 (1988).
38) M. Mansuripur, *J. Appl. Phys.*, **66**, 3731 (1989).
39) M. Mansuripur and M. F. Ruane, *IEEE Trans. Magn.* **MAG-22**, 33 (1986).
40) C. J. Lin and D. Rugar, *IEEE Trans. Magn.* **MAG-24**,

2311 (1988).
41 D. Rugar, H. J. Mamin and P. Guthner, *Appl. Phys. Lett.*, 55, 2588 (1989).

[Received October 15, 1990]

Masud MANSURIPUR

1977: BSEE in Electrical Engineering at Arya-Mehr University of Technology (Tehran, Iran).

1978: MS in Electrical Engineering at Stanford University.

1980: MS in Mathematics at Stanford University.

1981: PhD in Electrical Engineering at Stanford University.

During and after his graduate studies, he worked at the Xerox Palo Alto Research Center on erasable optical data storage materials and systems.

1982: Joined as a member of the faculty of the Electrical Engineering Department in Boston University.

1988: Joined as Associate Professor of the Optical Sciences Center in the University of Arizona.

Present: Associate Professor of the Optical Sciences Center in the University of Arizona.

Member of the Institute of Electrical and Electronics Engineers (IEEE) and Optical Society of America (OSA).

Research Field: Studies on magnetic and optical properties of amorphous materials with emphasis on thin film and multilayer structures. Computer simulations of micromagnetics and domain wall dynamics. Developing novel experimental methods for studying magnetic and optical properties of materials.

Roscoe C. GILES

1970: BA in Physics at the University of Chicago.

1975: PhD in Physics at Stanford University. Worked as post-doctoral fellow in theoretical particle physics at the Stanford Linear Accelerator Center and at the Center for Theoretical Physics at MIT and has been Assistant Professor of Physics at MIT.

Present: Professor of the Electrical, Computer and Systems Engineering Department of Boston University.

Member of the Boston University Center for Computational Science.

Member of the American Physical Society, Sigma Xi and Phi Beta Kappa.

Research Field: Large scale computer simulations of magnetic materials and on molecular dynamics. Developing massively parallel algorithms and applications.

George PATTERSON

1987: BS in Physics at MIT.

Present: Doctoral student in the Department of Physics at Boston University.

Research Field: Supercomputer simulations of magnetic materials. Simulations of rare earth-transition metal alloys and analysis of three dimensional topological structures in magnetic materials for vertical Bloch line memories.